Original article

# Unmixing and pigment identification using visible and short-wavelength infrared: Reflectance vs logarithm reflectance hyperspaces

Eva M. Valero [a], Miguel A. Martínez-Domingo [a], Ana B. López-Baldomero [a,*], Ana López-Montes [b], David Abad-Muñoz [b], José L. Vílchez-Quero [c]

[a] *Color Imaging Laboratory, Department of Optics, Faculty of Sciences, University of Granada, Avda. Fuentenueva s/n, Granada 18071, Spain*
[b] *Department of Painting, Faculty of Fine Art, University of Granada, Avda. Andalucia s/n, Granada 18071, Spain*
[c] *Research Group of Analytical Chemistry and Life Sciences, Department of Analytical Chemistry, Faculty of Sciences, University of Granada, Avda. Fuentenueva s/n, Granada 18071, Spain*

## ARTICLE INFO

## ABSTRACT

Hyperspectral imaging has recently consolidated as a useful technique for pigment mapping and identification, although it is commonly supported by additional non-invasive analytical methods. Since it is relatively rare to find pure pigments in aged paintings, spectral unmixing can be helpful in facilitating pigment identification if suitable mixing models and endmember extraction procedures are chosen. In this study, a subtractive mixing model is assumed, and two approaches are compared for endmember extraction: one based on a linear mixture model, and the other, nonlinear and Deep-Learning based. Two spectral hyperspaces are used: the spectral reflectance (R hyperspace) and the -log(R) hyperspace, for which the subtractive model becomes additive. The performance of unmixing is evaluated by the similarity of the estimated reflectance to the measured data, and pigment identification accuracy. Two spectral ranges (400 to 1000 nm and 900 to 1700 nm) and two objects (a laboratory sample and an aged painting, both on copper) are tested. The main conclusion is that unmixing in the -log(R) hyperspace with a linear mixing model is better than for the non-linear model in R hyperspace, and that pigment identification is generally better in R hyperspace, improving by merging the results in both spectral ranges.

© 2023 The Authors. Published by Elsevier Masson SAS on behalf of Consiglio Nazionale delle Ricerche (CNR).
This is an open access article under the CC BY-NC-ND license (http://creativecommons.org/licenses/by-nc-nd/4.0/)

## 1. Introduction

The conservation of cultural heritage is crucial to ensure its continued existence and value for future generations. In this context, the study of paintings is of great importance for their preservation and restoration [1–4].

For this purpose, the use of non-invasive techniques is generally preferred [2–4]. Spectral imaging techniques [5] allow both identification and mapping of pigments, which is used to understand the technique of the artist, the evolution of painted surfaces over time, to decide on the conservation strategies, and to detect restorations or forgeries [6,7].

Hyperspectral devices can measure the spectral reflectance of objects across different ranges: from UV (between 330 and 380 nm) through visible and near infrared (VNIR, up to 1000 nm) to short-wavelength infrared (SWIR, usually between 900 and 2500 nm). In the context of art conservation, different materials exhibit unique features within these ranges: varnishes have interesting properties in the UV [8], while pentimenti and underdrawings are detected in the SWIR [9], and pigments have distinctive features in the VNIR range [10]. In addition, hyperspectral imaging can detect and separate the components of pigment mixtures (spectral unmixing).

In spectral unmixing, a mixed spectrum is decomposed into their constituent spectra, or endmembers (EMs) [11], and their relative concentrations in the mixture are estimated. EMs represent the pure materials used to produce the mixtures, while the concentrations represent the proportion of each EM present in every

pixel of the image. Unmixing is then divided into two steps: EM extraction and concentration estimation.

The unmixing process is based upon mixing models that describe the physical processes that occur when different pigments are mixed. They can be classified as linear or non-linear. In linear models, the mixed spectrum is obtained from a linear combination of EMs weighted by the concentrations. It is commonly used in remote sensing [12–14] and it is assumed as an acceptable approximation in many real scenarios. Its assets are physical interpretability, computational tractability, and ease of implementation [15,16]. It has been used in the field of cultural heritage with promising results [17,18].

Nevertheless, when pigments are mixed, the individual components are not discernible with imaging technologies [19]. Therefore, these mixtures are better characterized by a non-linear model [20,21]. For instance, the Kubelka–Munk model describes the relationship between the absorption and scattering coefficients of incident light in highly light-scattering materials, requiring information about the optical properties of the materials studied [22]. It has been used in the cultural heritage domain as a proof of concept [23], but it is not extended due to memory requirements and computation times [6]. In remote sensing, non-linear unmixing is performed by parametric extensions of the linear model addressing the spectral variability found in the set of EM across different pixels [24] or considering different combinations within the set of EM [25]. These approaches do not incorporate the physical principles that underlie the Kubelka–Munk model. Recently, a generative Deep-Learning based model (DeepGun) was introduced for unsupervised unmixing [26] using low-dimensional representations of EMs in the latent space of the generative model. The network is re-trained for each scene and provides a set of EM for each pixel. This model performs better than the parametric non-linear extensions of the linear model, and it is not computationally expensive if subsampling techniques reduce the number of pixels in the spectral image.

Many studies have focused on obtaining robust, accurate and tractable unmixing algorithms [11]. Grillini et al. [17] explored various mixing models, finding that the subtractive model outperformed others. They tested the LIP (Logarithmic Image Processing) additive and LIP subtractive models but, to our knowledge, the simplest way to transform a subtractive into an additive model (taking the -log of the spectral reflectance data) has not yet been explored. This transformation can be especially interesting if the EM extraction models used are linear, like NFINDR [27] or Pixel Purity Index (PPI) [11].

After selecting the mixture model and performing EM extraction, the next step is pigment identification. This is usually done by linking each EM to a pigment within a reference library by using different metrics [28]. Ideally, the reference library should include a wide range of common pigments applied on a suitable ground layer, since some pigments become transparent in the near-infrared range [29]. Finding pure pigments in artworks is usually challenging, particularly when they undergo aging [21,30,31], weathering [32] or restoration processes [33], which makes the use of unmixing techniques especially appropriate. Also, the use of binders and varnishes can alter the spectral signature of a given pigment [34].

Several approaches have been proposed for spectral unmixing and pigment identification, like using the first and second derivative of the spectra [31,35,36], clustering [16], pattern-recognition algorithms [37], Neural Networks, and Deep Learning [6,23,38–41]. The ENVI spectral hourglass wizard has also been used [35,42], but it is slow and not fully automatic [29]. Achieving effective spectral unmixing still remains a challenging task.

Most studies use the VNIR range to perform spectral unmixing, pigment mapping and/or pigment identification

[7,17,18,23,29,31,35]. Some have used the SWIR range to perform pigment mapping [36,42,43], but not unmixing.

## 2. Research aim

In this study, a subtractive mixing model was used, which transforms into a linear mixing model in the -log(R) hyperspace. Our hypothesis is that linear EM extraction algorithms will benefit from the -log(R) hyperspace. The research question is if they can outperform non-linear models in R hyperspace. To answer this question, three EM extraction models were tested in R hyperspace. Then, two of them (linear mixing model-based algorithm and manual extraction) were tested in the -log(R) hyperspace. Apart from showcasing the success of simple solutions for challenging tasks, unmixing results in two spectral ranges and two different hyperspaces are analyzed, and the assets and drawbacks of each method/hyperspace/range are discussed.

## 3. Material and methods

### 3.1. Samples

Two main objects have been used: an auxiliary (reference) copper plate from which a checkerboard image was extracted, and the painting on copper with the inscription "Boceto di Pablo Veronese". These objects and the information extracted from them are described in the next two subsections.

### 3.1.1. Reference copper plate

The copper reference plate and the checkerboard image with reference pigments are shown in Fig. 1. The preparation used is in accordance with documented period techniques from the XVIth century [44–47]. The materials are preparation layers and pigments found in the painting [48]. The pigments (Kremer Pigmente GmBH) were bound with linseed oil and applied with a brush.

The unpolished copper plate (1 mm thickness) was cleaned with calcium carbonate and vinegar, and rubbed with ground garlic. Then, a layer of $CaSO_4$ powder bound with linseed oil was applied, and a preparation layer (P1) of Bone black (BB) mixed with Read Earth (REP) and Lead White (LW) bound with linseed oil. Then, the pigments and mixtures are deposited on the prepared surface. There are seven pure pigments: LW, Naples Yellow (NY), BB, Cinnabar (CN), Lapislazuli (LL), Azurite (AZ) and REP. Three more patches with mixtures are added: LL + LW, CN + LW, and the P1 mixture. Ten 32×32 pixel areas were extracted from the spectral image of the plate to build the reference checkerboard image shown in Fig. 1 (bottom).

### 3.1.2. Painting on copper

The copper plate was prepared specifically for a pigment identification test of a painting on copper with the inscription "Boceto di Pablo Veronese", a Maternity containing the Virgin, St. Joseph and Jesus. This painting was studied using X-Ray Fluorescence (XRF) and X-Ray Diffraction (XRD) techniques [48], concluding that it contained five pigments: LW, BB, LL, NY and CN.

The dimensions of the painting are 13.5 × 17.5 cm, and it has recently been restored. In the restoration process, the chromatic reintegration was made with Maimeri pigments ochre, natural earth, toasted ochre, Naples yellow (Lead antimonium), Zinc white, Lapislazuli, and Cadmium Red from Windsor Newton. A new layer of varnish was applied (Lefranc-Bougeois satined with UV protection). An RGB image obtained with three spectral bands ($R = 605$ nm, $G = 535$ nm and $B = 430$ nm) is shown in Fig. 2, with several 3 × 3 pixels areas marked in bright yellow, which were used to build the manual extraction (MEx) EM library as explained in Section 3.3.2.

E.M. Valero, M.A. Martínez-Domingo, A.B. López-Baldomero et al.

*Journal of Cultural Heritage 64 (2023) 290–300*



**Fig. 1.** (Top) Reference copper plate. Reference checker areas extracted are highlighted with red squares. (Bottom) Reference checkerboard image containing areas 1–10 (for interpretation of the references to color in this figure legend, the reader is referred to the web version of this article).



**Fig. 2.** Restored painting used in this study, with the 3 × 3 pixels areas used for manual EM extraction marked in bright yellow.

### 3.2. Spectral image capture and reference library

We used two cameras from Resonon Ltd. coupled to a linear stage to capture the reference copper plate and the painting. The first (Pika L) covers the spectral range from 380 to 1080 nm (VNIR range). The second (Pika IR+) covers from 888 to 1732 nm (SWIR range). We cropped the extremes of the range, obtaining finally 121 bands in VNIR and 161 bands in SWIR. The sampling interval was 5 nm for both ranges.

After capturing the reference plate, a reference library of eight spectra for pigment identification (REFL from now on) was built using the average reflectance of 30×30 pixels areas within the patches labelled as 1–7 and 10 in Fig. 1 top. The areas used in REFL were different from those in the reference checkerboard image shown in Fig. 1 bottom. All image processing and unmixing modelling has been performed using Matlab® software.

In Fig. 3, the spectral reflectances from the REFL in both VNIR and SWIR ranges are shown. The spectra differ both in shape and scale.

### 3.3. Unmixing methods

The process of unmixing often takes two steps: EM extraction (Section 3.3.2) and concentration estimation (Section 3.3.1).

#### 3.3.1. Concentration vector estimation and reflectance hyperspaces

Two mixing models have been used depending on the hyperspace. In the R hyperspace, the subtractive model [49] was used. The spectra of i EMs are multiplied consecutively, elevated to the
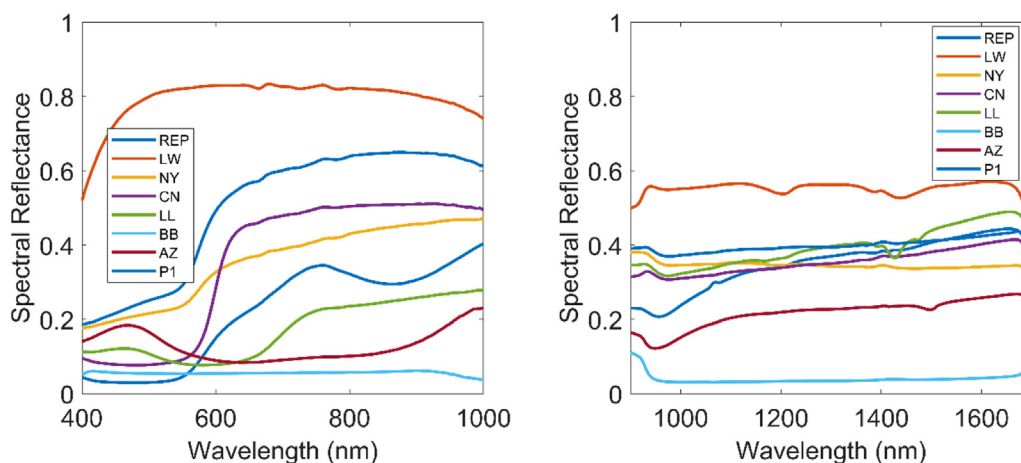
**Fig. 3.** (Left) REFL spectra in the VNIR range. (Right) REFL spectra in the SWIR range.

power of the concentrations (Eq. (1)).

$$Y = \prod_{i=1}^{q} \rho_i^{\alpha_i} \qquad (1)$$

where, Y is the reflectance of the mixture, $q$ is the number of candidate EMs, $\rho_i$ is the reflectance of the $i$th EM, and $\alpha_i$ its concentration.

Some blind EM estimation algorithms, like NFINDR [27] and FIPPI (Fast Iterative Pixel Purity Index) [50], are based on a linear model. This fact prompted the idea of introducing the -log(R) hyperspace for performing unmixing. In -log(R) hyperspace, the reflectance of a subtractive mixture transforms into a linear combination of EMs, as shown in Eq. (2) [51].

$$Y = \sum_{i=1}^{q} \alpha_i \rho_i \qquad (2)$$

The goal of spectral unmixing is retrieving the vector of concentrations ($C = (\alpha_1, \alpha_2, \ldots \alpha_q)$) from the reflectance of the mixture (Y) and the library of candidate EMs ($E = (\rho_1, \rho_2, \ldots \rho_{iq})$). For this, a constrained optimization method is used. In this study, the fmincon function with the interior point algorithm [52] implemented in Matlab® was used. The constraints are non-negativity ($\alpha_i > 0, \ \forall \ i$), and sum-to-one ($\sum_{i=1}^{q} \alpha_i = 1$).

For the cost function, usually spectral metrics are used, such as Mean Square Error (MSE [17]) or the complement of the Goodness-of-Fit coefficient (cGFC [53]), related to the Spectral Angle Mapper metric (SAM). MSE is influenced by offset differences, and cGFC only accounts for shape differences. A perfect match would have zero MSE and cGFC values. Our cost function (M) merges both together (Eq. (3)).

$$M = cGFC + \beta \cdot MSE \qquad (3)$$

$\beta$ is a scaling parameter to balance the contribution of both sub-metrics to the final combined metric. In a preliminary experiment, the optimal value for $\beta$ parameter to ensure equal contribution of both metrics was found to be $\beta = 1.0936$.

Summarizing, both R and -log(R) hyperspaces, each with its unmixing model (subtractive and additive, respectively), are used for the checkerboard image with different EM libraries in VNIR and SWIR ranges. The best performing method according to the criteria explained in Section 3.5 is selected for analyzing the painting on copper.

### 3.3.2. EM extraction

EMs can be obtained by blind separation using different algorithms, like Pixel Purity Index (PPI [54,55]), or Fast Iterative PPI (FIPPI [50]) and NFINDR [27]. The first two use a heuristic approach. NFINDR is geometry-based, searching for members of a simplex hyperspace that can cover the input data [56]. NFINDR and PPI assume the presence of at least one pure pixel per EM in the data [11]. The NFINDR and DeepGun [26] methods have been selected for this study as representative instances of automatic EM extraction methods with different design strategies. The Matlab® libraries of ENVI integrated package for NFINDR, and the code provided by the authors of DeepGun [57] was used with the default parameters adapted to the number of extracted EM. For DeepGun, the extraction was performed only in (R) hyperspace, because the DeepGun algorithm is non-linear in R hyperspace.

Other possibility is to extract the library directly from the painting, out of representative areas including mixed pigments (Manual Extraction or MEx method) [35]. Five 3 × 3 pixel representative areas (shown in Fig. 2) of black, blue, red, white, and yellowish colors were extracted from the image of the painting. The spectra were averaged to build the MEx_p library. The MEx_p library is very likely constituted by mixtures and not pure EMs, but our hypothesis is that this library will provide more accurate concentration estimations since it is obtained directly from the painting. In any case, the MEx_p EMs will be used for pigment identification using the REFL spectra shown in Fig. 3 as reference.

Summarizing, we have seven libraries in R hyperspace for each spectral range. Four of them are extracted from the copper reference board: REFL, which will only be used for pigment identification, and other three (with 7 EM), which will be used for unmixing: the NFINDR library (NFDL), the DeepGun library (DeGu), and the Manual Extraction library (MEx), which includes the same pure pigments as REFL but extracted from different areas. The remaining three libraries (with 5 EM) are extracted from the painting spectral image: NFDL_p, DeGu_p and MEx_p. The goal is not to find the best extraction method in absolute terms, but to choose three representative instances of extraction methods to showcase the proposed methodology.

In -log(R) hyperspace, for each spectral range we have the two NFINDR libraries with 7 and 5 EMs, and the two M_Ex libraries for concentration estimation.

### 3.4. Pigment identification

The method consists of two parts: the first, computation of a combined distance metric between each pair of spectra from the
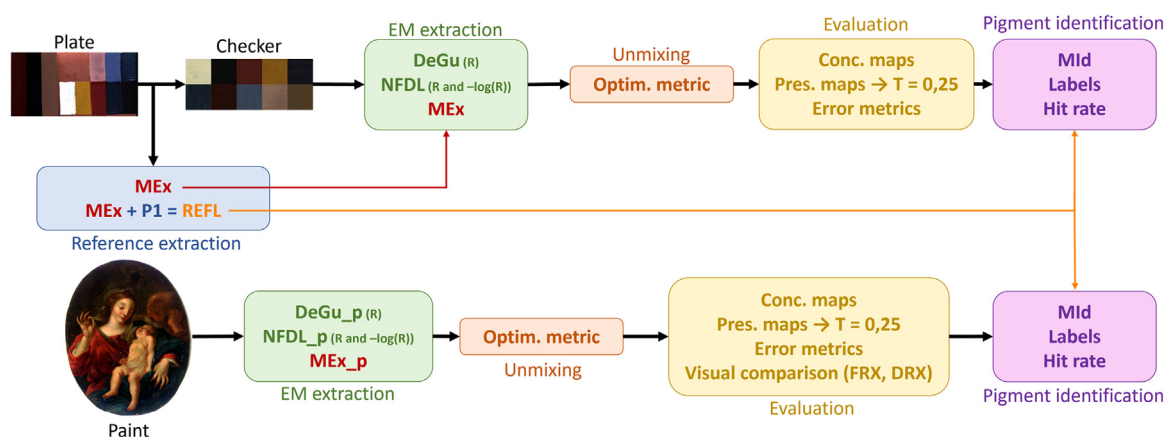
**Fig. 4.** Workflow of the steps used in the different phases of this study.

candidate library and REFL. The metric for the VNIR spectra is shown in Eq. (4):

$$MId = cGFC + 0.5MSE + 0.02\Delta E_{00} \qquad (4)$$

The coefficients are obtained assuming the following tolerances for the three components of the metric: 0.01 for cGFC, 0.02 for MSE and 0.5 for $\Delta E_{00}$. They ensure that all the factors would contribute equally to the metric value in an acceptable reflectance match. The tolerance values are based on experience and correspond with tolerances found in the literature for spectral estimation [53]. The metric contains a color difference term because color can be relevant for pigment identification, while both scale and shape differences in spectra are also accounted for. The combined metric in the SWIR range contains only the two first factors. The lower the MId value, the higher the similarity between the compared spectra.

The second part is the label assignment: the REFL label corresponding to the pigment with the minimum metric value is assigned to each EM.

Finally, the hit rate of the pigment identification process is calculated as the percentage of correctly identified pigments.

### 3.5. Evaluation of results

The evaluation of the results obtained is based on three factors:

a) Spectral reconstruction: the similarity between estimated spectra and the original spectra, assessed separately by the three metrics that form MId (Eq. (4)).
b) Visual assessment: using concentration or presence maps. The data shown in Ref. [48] will be used to determine if the maps are plausible for the painting.
c) Hit rate: from pigment identification.

Fig. 4 shows the workflow of the methods to clarify the procedures described in the previous subsections.

## 4. Results and discussion

### 4.1. Copper reference plate

In this section, a summary of the EM extraction and unmixing results for the spectral data of the checker reference image (Fig. 1 bottom) is shown. Extended results are presented in the supplementary material for briefness.

### 4.1.1. Unmixing results
*4.1.1.1. Spectral reconstruction quality.* Regarding R hyperspace, the best results in terms of cGFC, RMSE and $\Delta E_{00}$ values are obtained

with the MEx library (see Supplementary Material for numerical results). The second-best corresponds globally to NFDL, which is close to DeGu in most spectral metrics. In -log(R) hyperspace, the best results belong to NFDL in all metrics (VNIR range), and in cGFC in the SWIR range. In general, the -log(R) transformation is beneficial for the NFDL in both ranges, which points to the importance of ensuring correspondence between the mixing models in EM extraction and concentration estimation.

Comparing both spectral ranges, the estimation of the image reflectances is more accurate in the SWIR range. This is expected because the SWIR reflectances tend to be flatter and with less scale changes than the VNIR reflectances.

*4.1.1.2. Concentration and presence maps.* The concentration maps show, in grayscale, the concentration of the endmembers for each pixel of the checkerboard reference image, ranging between 0 (black) and 1 (white). In Fig. 5, the concentration maps corresponding to the three libraries tested in the VNIR range and R hyperspace are shown, along with the labeled checkerboard reference image. For NFDL and DeepGun, the EMs are not directly mapped into pigments, as it happens for the MEx library. But sometimes correspondences can be induced from the concentration maps' results. For instance, if an EM concentration map shows significant presence of the EM in patches 5 (LL) and 8 (LL+LW), with higher concentration values in patch 5, and just negligible traces in the other patches, it is safe to assume that this EM corresponds to the LL pigment.

Even for the MEx library, the results of the unmixing as judged by the concentration maps shown in Fig. 5 (right column) are not completely satisfactory. For instance, EM3 (NY) is not detected with a high concentration in patch four, and the two red pigments (REP and CN, EM1 and EM4) tend to be confused to a certain extent. On the other hand, LW is correctly identified as present in the three mixed patches (8, 9 and 10) in EM2 concentration map. The NFDL concentration maps (Fig. 5, left column) present certain similarities with the MEx results. For instance, EM4 concentration map in NFDL is rather similar to EM2 (LW) for manual extraction, and EM1 from NFDL is similar to EM4 (CN) of the MEx library. The DeepGun concentration maps (Fig. 5, middle column) show relatively good results for EM4 (presumably corresponding to LL), EM6 (which has similar appearance to the LW, MEx EM2, concentration map) and EM2 (presumably REP). However, EM1 (presumably AZ) is confused with the LL present in patch 8, and the other three concentration maps (EM3, EM5 and EM7) are very much alike.

In the SWIR range, the concentration maps reflect less similarity between NFINDR and MEx libraries results. In general, none of the libraries is able to correctly reproduce the real contents of the reference image.

E.M. Valero, M.A. Martínez-Domingo, A.B. López-Baldomero et al.

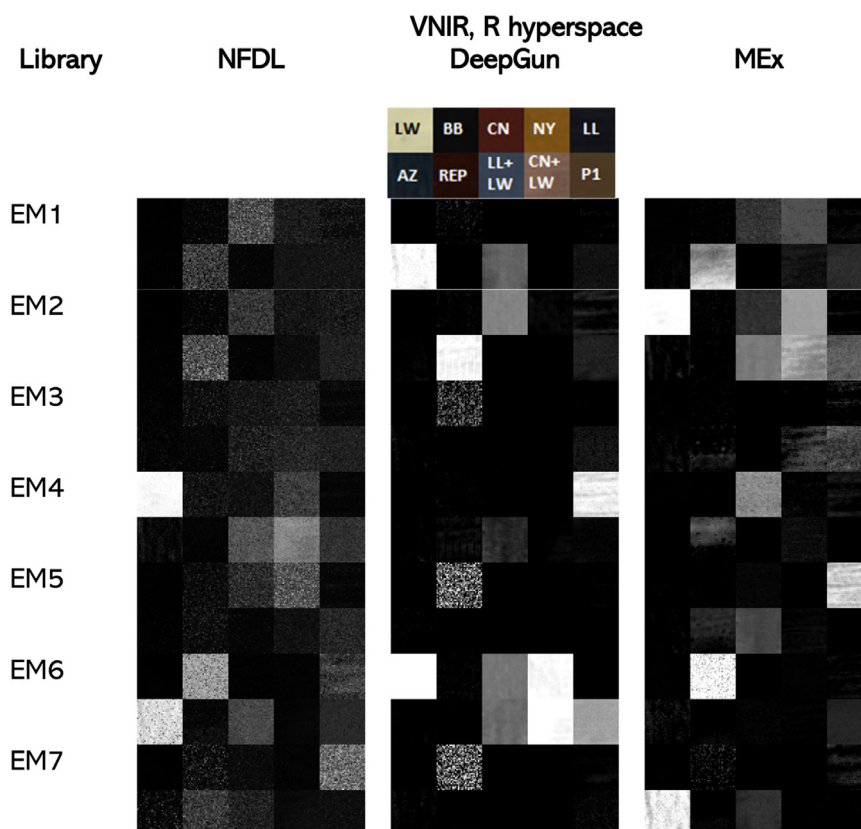Journal of Cultural Heritage 64 (2023) 290–300



**Fig. 5.** VNIR range concentration maps in R hyperspace for the checker reference image and the three EM libraries tested. EMX stands for Endmember X.

Regarding the concentration maps in the -log R hyperspace, the best results correspond to the NFDL in the VNIR range, which clearly benefits from the change to an additive model.

Summarizing, neither concentration maps nor presence maps can capture accurately enough the pigment distribution in the checker reference image with any of the three libraries tested or in any of the spectral ranges, although some of the libraries produce results that are reasonable if not entirely accurate. For instance, consistent results were offered by NFDL in -log(R) hyperspace (see figures in Supplementary Material). In general, SWIR range tends to offer less consistent results.

### 4.1.2. Pigment identification results

The best results are obtained by the NFDL in the SWIR range and R hyperspace, with a 100 % hit rate in pigment identification, and maximum MId values very near the tolerance of 0.02 for all EMs. The second-best results correspond to NFDL -log(R) hyperspace in the VNIR range, with a hit rate of 85.7 %. DeGu obtains at most four out of seven pigments in both ranges. Despite the good unmixing results for -log(R) hyperspace in the VNIR range and NFINDR, the pigment identification is slightly better in the SWIR range and R hyperspace for this library. This suggests that it is convenient to include both ranges in the pigment identification procedure.

### 4.1.3. Proposed method for analysis of the painting on copper

Given the results for the copper reference plate with known and regular pigment distribution, the following method will be employed for obtaining concentration/presence maps and pigment identification for the painting on copper:

a) Use the -log(R) hyperspace and NFDL_p with 5 EMs extracted from a subsampled spectral image (1:2 ratio) to obtain the con-

centration and presence maps. The subsampling allows to reduce the computation time required for the unmixing.

b) Use the REFL library extracted from the copper plate to perform pigment identification in both R and -log(R) hyperspaces with NFDL_p.

In this case, we expect lower rates of success in the pigment identification phase, because the painting has been aged for a long period of time and the raw materials used for the pigments and binders might not be exactly the same in the painting and reference copper plate.

### 4.2. Painting on copper

Although we will show the results corresponding to the method proposed in Section 4.1.3, for brevity, a complete analysis using DeGu_p and MEx_p libraries was carried out. The results of these libraries will be commented on only when they outperform NFDL_p.

### 4.2.1. Unmixing results

4.2.1.1. Extracted EM libraries. In Fig. 6, the NFDL_p libraries in VNIR and SWIR range in -log(R) hyperspace are shown along with the MEx_p library.

The NFDL_p EMs are clearly higher in scale than MEx_p EMs, and they tend to be less flat in the SWIR range.

4.2.1.2. Spectral reconstruction quality. In Table 1, the quality metrics are shown for the NFDL_p (based on the NFINDR algorithm and a linear mixing model), DeGu_p (based on Deep Learning for endmember extraction and a non linear model) and MEx_p (based on manual EM extraction) libraries in both spectral hyperspaces and both spectral ranges.
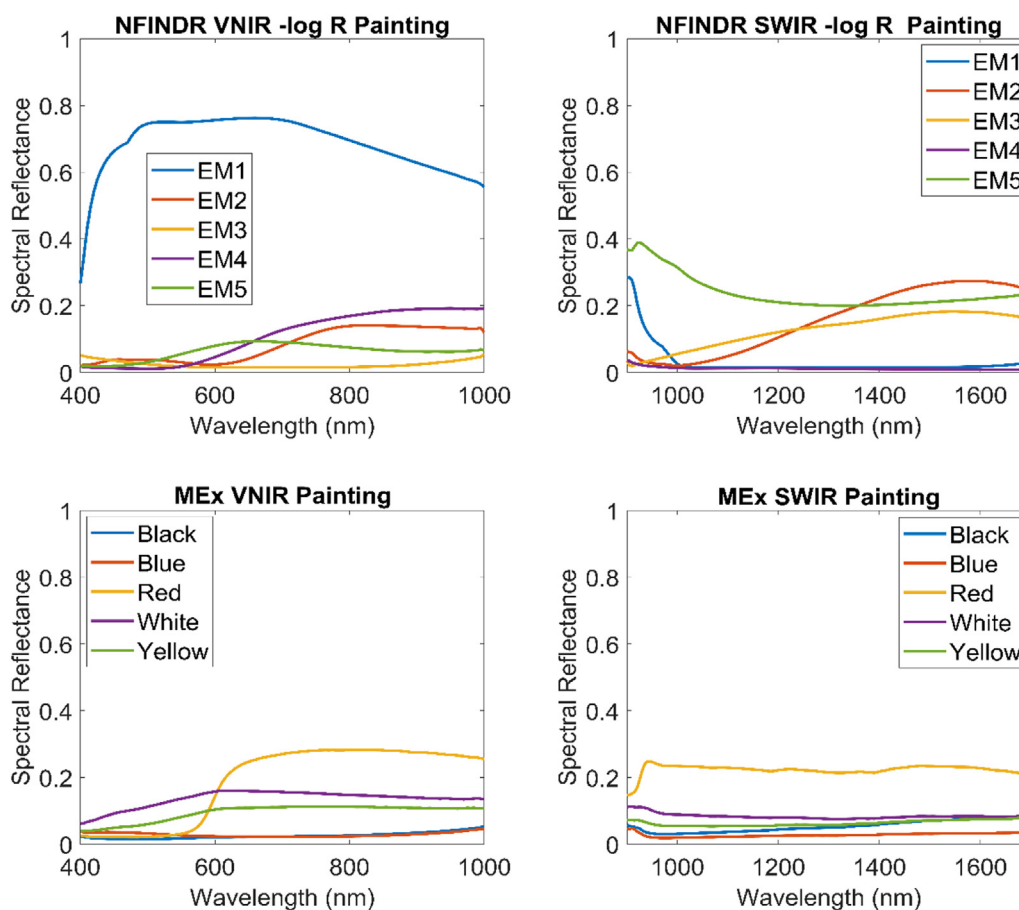
**Fig. 6.** VNIR range libraries (left) and SWIR range libraries (right) extracted with NFINDR (upper row) and by Manual Extraction MEx_p (Lower row) from the painting on copper. EMX stands for Endmember X.

**Table 1**
Spectral reconstruction quality metrics for the two EM libraries in VNIR and SWIR, and in both hyperspaces. The best results for each metric and spectral range are in bold.

| Library | Hyperspace | Mean cGFC (STD) | Mean MSE (STD) | Mean $\Delta E_{00}$ (STD) | Spectral range |
|---|---|---|---|---|---|
| NFDL_p, MEx_p, DeGu_p | R | 0.0104 (0.010) | 0.0743 (0.0309) | 12.64 (5.11) | VNIR |
| | | **0.0025 (0.0036)** | **0.0136 (0.0146)** | **4.16 (2.29)** | |
| | | 0.0037 (0.0036) | 0.0324 (0.0270) | 6.22 (4.39) | |
| NFDL_p, MEx_p | -log(R) | 0.0065 (0.0095) | **0.0055 (0.0047)** | 3.81 (2.48) | |
| | | **0.0051 (0.0074)** | 0.0076 (0.0125) | **3.69 (2.50)** | |
| NFDL_p, MEx_p, DeGu_p | R | 0.0032 (0.0103) | 0.0108 (0.0121) | – | SWIR |
| | | 0.0051 (0.0074) | **0.0076 (0.0125)** | – | |
| | | **0.0016 (0.0030)** | 0.0244 (0.0213) | – | |
| NFDL_p, MEx_p | -log(R) | **0.0035 (0.0055)** | **0.0047 (0.0100)** | – | |
| | | 0.0090 (0.0267) | 0.0064 (0.0010) | – | |

In the VNIR range, the best results (this is, the lowest values of spectral metrics) correspond to MEx_p in -log(R) hyperspace, although the best cGFC value is found in R hyperspace for this library. The metric values found for NFDL_p in -log(R) hyperspace are close to the MEx_p library, with the lowest MSE values. However, in R hyperspace the NFDL_p estimation is clearly worse than MEx_p estimation, and DeGu_p outperformed NFDL but not MEx_p.

In the SWIR range, the best results for MSE are found again for NFDL_p in -log(R) hyperspace, and for cGFC in DeGu_p in R space. In general, the quality of the estimation is acceptable or remarkably good, depending on the hyperspace and range, save for NFDL_p in VNIR range and R hyperspace.

The beneficial effect for the scale sensitive metrics (MSE and $\Delta E_{00}$) of the -log(R) hyperspace transformation is remarkable, and

overall, the SWIR estimated spectra are closer to the original according to the spectral metrics, which is expected because they have lower maximum values.

*4.2.1.3. Presence and concentration maps.* In Fig. 7, the concentration maps for the NFDL_p and MEx_p libraries in -log(R) hyperspace and VNIR range are shown. The order of the MEx_p EMs corresponds to Fig. 6.

According to the XRF and XRD results [48], LL can be found both in the Virgin's mantle and in the background. This is corroborated by the VNIR range concentration maps EM1 and EM2 for MEx_p (second row), and EM3 for NFDL_p (first row of Fig. 7).

The CN pigment is found in the Virgin's dress and in the carnations, which is corroborated by MEx_p EM3 (second row) and NFDL_p EM4 (first row). The LW is found in the carnations and
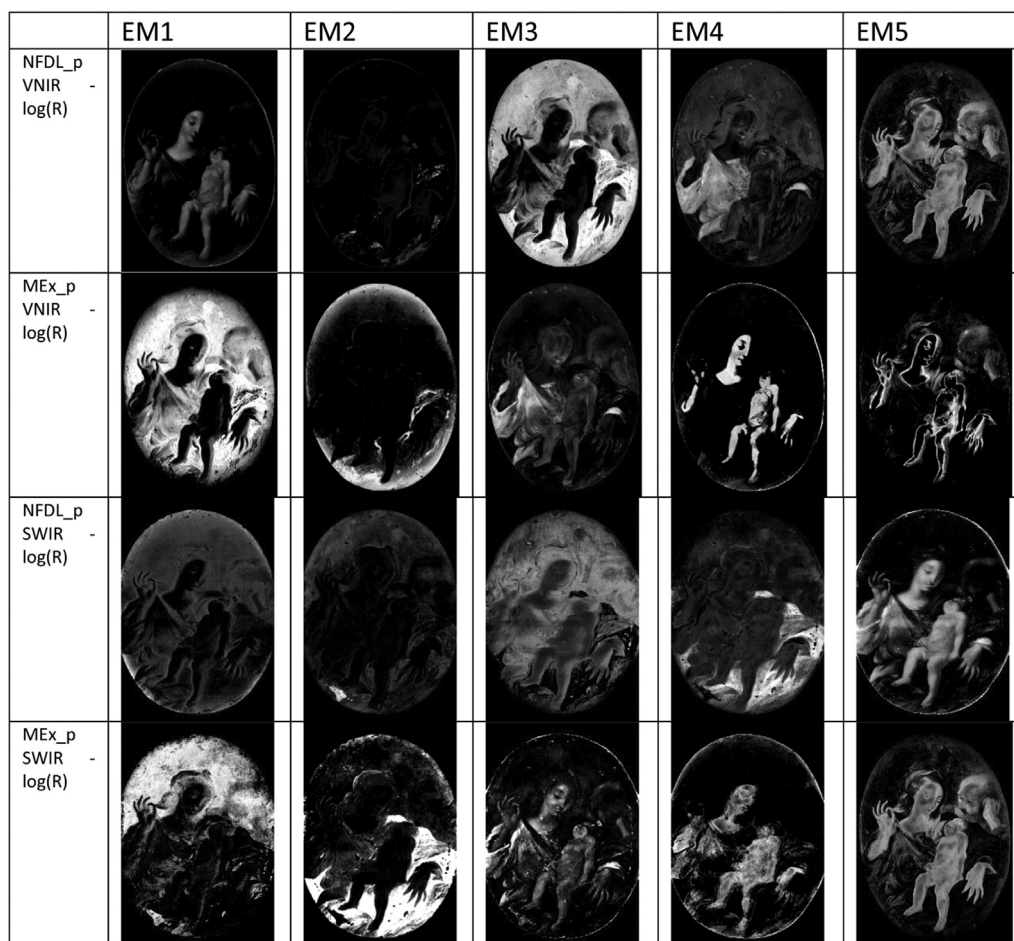
**Fig. 7.** Concentration maps in -log(R) hyperspace corresponding to the libraries shown in Fig. 6. First row: NFDL_p VNIR range; second row: MEx_p VNIR range; third row: NFDL_p SWIR range; fourth row: MEx_p SWIR range.

in the Virgin's chemise sleeves, which is corroborated by MEx_p EM4 (second row) and NFDL_p EM1 (first row). The BB pigment is found in the shadowed areas and in the background, which would be supported by MEx_p EM1 (second row) and NFDL_p EM3 (first row). And finally, the NY pigment is found in some parts of the carnations and in the Child's cloth. This would correspond to EM5 in both libraries. The VNIR results are consistent, with some trend to confuse background with LL pigment in some areas for MEx_p.

In the SWIR range, there are some remarkable findings: the first is that the confusion between BB and LL is less marked for MEx_p (see EM1 and EM2 in the fourth row of Fig. 7). The second is that for NFDL_p, the LW and CN results are intermingled in EM5 concentration map (third row), while this does not happen for MEx_p (see EM3 and EM4 in the fourth row). And the third is that the NY does not appear clearly in the NFDL_p EMs, while it seems to appear in EM5 for MEx_p (fourth row). The NY pigment is the least present in the painting and appears mostly in mixtures. Overall, the results for the MEx_p library in the SWIR are more consistent, even if the estimation quality is lower than for NFDL_p.

In Fig. 8, the presence maps with a threshold of 0.25 are shown for both libraries and both ranges, in -log(R) hyperspace.

Considering the inherent limitations of the unmixing techniques, the presence map results are rather satisfactory and consistent with the pointwise XRF and XRD results [48]. It is found out that the carnations are a mixture of three EMs, one of them present as well in the Virgin's dress. Or that the Virgin's veil is also a mixture of at least three EMs.

### 4.2.2. Pigment identification results

In Table 2, the results from the pigment identification for NFDL_p using REFL library as reference are shown.

The best result is obtained for R hyperspace and SWIR range with a hit rate of 80 %, failing to identify the LL pigment. However, if one considers the union of the two ranges, there would be seven pigments, of which only one is not present in the painting (AZ). This union strategy seems to work better also for the -log(R) hyperspace, which would result in six pigments, of which one is not present in the painting (AZ). These results are of course condi-

**Table 2**
Pigment identification results for NFDL_p, using the copper reference REFL library as reference.

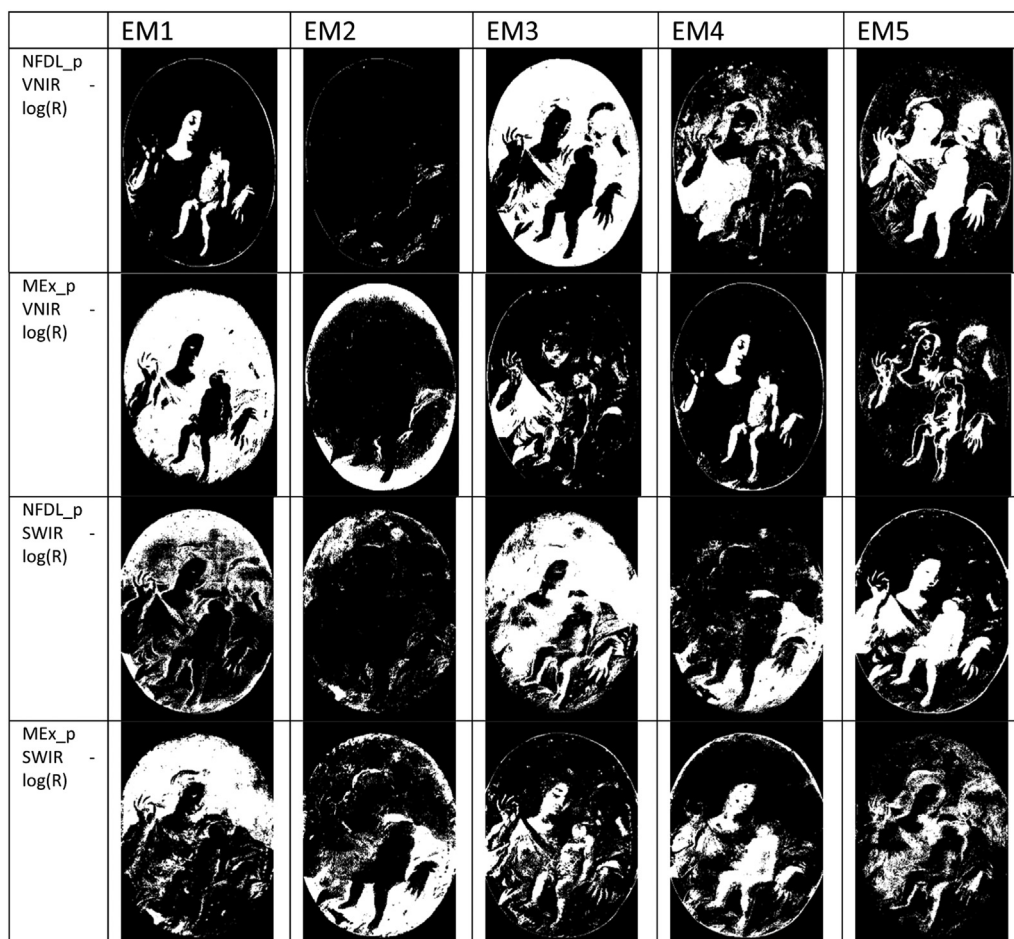| Library | Hyperspace | Range | Assigned labels | Hit rate | MId range |
|---------|-----------|-------|-----------------|----------|-----------|
| NFDL_p | **R** | **VNIR** | LL, REP, NY, REP, BB | 60 | 0.13–0.27 |
|  | -log(R) |  | LW, BB, BB, REP, BB | 40 | 0.11–0.41 |
|  | **R** | **SWIR** | **LW, CN, AZ, NY, BB** | **80** | **0.023–0.15** |
|  | -log(R) |  | BB, AZ, AZ, BB, NY | 40 | 0.06–0.28 |

**Fig. 8.** Presence maps with a threshold of 0.25, corresponding to the libraries shown in Fig. 6. Upper row: NFDL_p -log(R) VNIR range; second row: MEx_p -log(R) VNIR range; third row: NFDL_p -log(R) SWIR range; fourth row: MEx_p -log(R) SWIR range.

tioned by the very restricted and specific set of pigments used as reference.

Regarding the MId range values, the NFDL_p obtains the lowest value (0.023–0.15) for SWIR and R hyperspace. The results suggest that the SWIR range is more reliable than the VNIR range, in agreement with the hit rate values. None of the other libraries obtain better identification results than NFDL_p.

## 5. Conclusions

In this study, different unmixing techniques are applied for pigment detection and identification in two spectral ranges: VNIR and SWIR. The unmixing methods have been selected with the aim to compare two different methodologies: using a non-linear Deep-Learning based method in R space, and a linear classical method in -log(R) space.

A reference palette has been prepared, containing the pigments present in an oil painting on copper with the inscription "Boceto di Pablo Veronese" on the back, plus AZ (not present in the painting) and additional patches with mixtures.

The proposed methodology to analyze the painting has been selected using the results obtained with a reference checkerboard image obtained from this palette. For this image, the -log(R) hyperspace unmixing results are satisfactory for the NFDL library in VNIR range in terms of concentration maps and scale dependent quality metrics, although slightly worse for the shape-sensitive cGFC metric. The pigment identification results are also successful.

The method was applied to the restored painting on copper using NFDL_p in both R and -log(R) hyperspaces and in both spectral ranges. NFDL_p was able to provide plausible results for the concentration and presence maps in the VNIR range. NFDL_p in R hyperspace (SWIR range) was the most successful method for pigment identification. By merging the results of both ranges, the identification would be complete, although AZ was also identified as present in the painting. This supports the usefulness of the SWIR range both for unmixing and pigment identification in artworks.

The results show that, even with unsophisticated techniques (a classical linear algorithm like NFINDR), for some instances it is possible to obtain satisfactory results using only spectral information for analysis of naturally aged artworks on a somewhat unusual support like copper.

It is crucial to have adequate reference auxiliar pigment palettes for pigment identification using spectral reflectance information, as stated in other studies [29]. The main limitations of the proposed methodology are in pigment identification in the painting, due to the intrinsic differences between the reference pigments (new) and the painting pigments (aged). Although ageing can be modelled to some extent [58] or light-induced pigment degradation can be used [31], multiple variables are involved. The natural aging process changes the pigment spectral shape differently based on composition, light exposure, and environmental factors. In many cases, these specific factors are unknown, adding complexity to the identification task. The use of painting techniques which involve

very thin layers of pigment, like glazing, must also be considered, and will be taken into account in future studies.

It is worth spending additional effort in refining spectral imaging and unmixing methods so that they can perform on par with alternative techniques without requiring a priori information. One limitation is the influence of the preparation techniques, binding agents, varnish, and ageing on the reflectance spectra. A multivariate modelling of the changes introduced by all these factors could lead to more accurate results for stand-alone spectral information-based pigment identification in the future.

## Funding

## Supplementary materials

Supplementary material associated with this article can be found, in the online version, at doi:10.1016/j.culher.2023.10.016.

## References

[1] B. Grabowski, W. Masarczyk, P. Głomb, A. Mendys, Automatic pigment identification from hyperspectral data, J. Cult. Herit. 31 (2018) 1–12, doi:10.1016/j.culher.2018.01.003.

[2] B. Brunetti, C. Miliani, F. Rosi, et al., Non-invasive investigations of paintings by portable instrumentation: the MOLAB experience, Top. Curr. Chem. (Z) 374 (2016) 10, doi:10.1007/s41061-015-0008-9.

[3] M.P. Colombini, I. Degano, A. Nevin, Analytical Chemistry for the Study of Paintings and the Detection of Forgeries, Springer International Publishing AG, 2022 Cham.

[4] B. Borg, M. Dunn, A. Ang, C. Villis, The application of state-of-the-art technologies to support artwork conservation: literature review, J. Cult. Herit. 44 (2020) 239–259, doi:10.1016/j.culher.2020.02.010.

[5] K. Martinez, High resolution digital imaging of paintings: the vasari project, Microcomput. Inf. Manag. 8 (1991) 277–283.

[6] N. Rohani, E. Pouyet, M. Walton, O. Cossairt, A.K. Katsaggelos, Pigment unmixing of hyperspectral images of paintings using deep neural networks, in: Proceedings of the ICASSP, IEEE, May 2019, pp. 3217–3221. https://ieeexplore.ieee.org/document/8682838. Available from:.

[7] F. Grillini, J.B. Thomas, S. George, VisNIR pigment mapping and re-rendering of an experimental painting, J. Int. Colour Assoc. 26 (2021) 3–10.

[8] A. Pelagotti, L. Pezzati, N. Bevilacqua, V. Vascotto, V. Reillon, C. Daffara, A study of UV fluorescence emission of painting materials, Proc. Art 5 (2005) 1–14.

[9] M. Strojnik, G. Paez, A. Ortega, Near IR diodes as illumination sources to remotely detect under-drawings on century-old paintings, in: Proceedings of the SPIE, 8011, 2011, pp. 1931–1936.

[10] M.T. Eismann, Hyperspectral Remote Sensing, SPIE Press, 2012 Bellingham, Washington DC.

[11] J.M. Bioucas-Dias, A. Plaza, N. Dobigeon, et al., Hyperspectral unmixing overview: geometrical, statistical, and sparse regression-based approaches, in: Proceedings of the JSTARS, 5, 2012, pp. 354–379, doi:10.1109/JSTARS.2012.2194696.

[12] J.M. Bioucas-Dias, A variable splitting augmented lagrangian approach to linear spectral unmixing, in: Proceedings of the IEEE, 2009, pp. 1–4. https://ieeexplore.ieee.org/document/5289072. Apr 29Available from:.

[13] X. Song, X. Jiang, X. Rui, Spectral unmixing using linear unmixing under spatial autocorrelation constraints, in: Proceedings of the IGARSS, IEEE, 2010, pp. 975–978. https://ieeexplore.ieee.org/document/5649735. JulAvailable from:.

[14] S. Stagakis, T. Vanikiotis, O. Sykioti, Estimating forest species abundance through linear unmixing of CHRIS/PROBA imagery, ISPRS J. Photogrammetry Remote Sens. 119 (2016) 79–89, doi:10.1016/j.isprsjprs.2016.05.013.

[15] G. Zhang, S. Mei, B. Xie, et al., Spectral variability augmented sparse unmixing of hyperspectral images, TGRS 60 (2022) 1–13, doi:10.1109/TGRS.2022.3169228.

[16] M. Nie, Z. Liu, X. Li, et al., Novel method for hyperspectral unmixing: fuzzy c-means unmixing, Sens. Rev. 36 (2016) 184–192, doi:10.1108/SR-05-2015-0077.

[17] F. Grillini, J. Thomas, S. George, Comparison of imaging models for spectral unmixing in oil painting, Sensors 21 (2021) 2471, doi:10.3390/s21072471.

[18] Deborah H., Ulfarsson M.O., Sigurdsson J. Fully constrained least squares linear spectral unmixing of the scream (verso, 1893). WHISPERS. IEEE; Mar 24, 2021:1–5. Available from: https://ieeexplore.ieee.org/document/9484037.

[19] F. Grillini, J. Thomas, S. George, Linear, subtractive and logarithmic optical mixing models in oil painting, 2020 Gjøvik, Norway.

[20] D.R. Duncan, The colour of pigment mixtures, Proc. Phys. Soc. 52 (1940) 390, doi:10.1088/0959-5309/52/3/310.

[21] S. Lyu, D. Meng, M. Hou, S. Tian, C. Huang, J. Mao, Nonlinear mixing characteristics of reflectance spectra of typical mineral pigments, Minerals 11 (2021) 626 (Basel), doi:10.3390/min11060626.

[22] H. Yang, S. Zhu, N. Pan, On the Kubelka–Munk single-constant/two-constant theories, Textile Res. J. 80 (2010) 263–270, doi:10.1177/0040517508099914.

[23] N. Rohani, E. Pouyet, M. Walton, O. Cossairt, A.K. Katsaggelos, Nonlinear unmixing of hyperspectral datasets for the study of painted works of art, Angew. Chem. (Int. Ed.) 57 (2018) 10910–10914, doi:10.1002/anie.201805135.

[24] L. Drumetz, M. Veganzones, S. Henrot, R. Phlypo, J. Chanussot, C. Jutten, Blind hyperspectral unmixing using an extended linear mixing model to address spectral variability, IEEE Trans. Image Process. 25 (2016) 3890–3905, doi:10.1109/TIP.2016.2579259.

[25] J. Nascimento, G. Martín, Nonlinear spectral unmixing, in: Data Handling in Science and Technology, Vol 32, Elsevier, 2019, pp. 151–166.

[26] R.A. Borsoi, T. Imbiriba, J.C.M. Bermudez, Deep generative endmember modeling: an application to unsupervised spectral unmixing, TCI 6 (2020) 374–384, doi:10.1109/TCI.2019.2948726.

[27] M.E. Winter, N-FINDR: an algorithm for fast autonomous spectral end-member determination in hyperspectral data, in: Imaging Spectrometry, 3753, 1999, pp. 266–275, doi:10.1117/12.366289.

[28] D.J. Mandal, M. Pedersen, S. George, H. Deborah, C. Boust, An experiment-based comparative analysis of pigment classification algorithms using hyperspectral imaging, J. Imaging Sci. Technol. (2023) 30403–30418, doi:10.2352/J.ImagingSci.Technol.2023.67.3.030403.

[29] T. Kleynhans, D.W. Messinger, J.K. Delaney, Towards automatic classification of diffuse reflectance image cubes from paintings collected with hyperspectral cameras, Microchem. J. 157 (2020) 104934, doi:10.1016/j.microc.2020.104934.

[30] J. van der Weerd, A. van Loon, J.J. Boon, FTIR studies of the effects of pigments on the aging of oil, Stud. Conserv. 50 (2005) 3–22, doi:10.1179/sic.2005.50.1.3.

[31] I.M. Ciortan, T.G. Poulsson, S. George, J.Y. Hardeberg, Tensor decomposition for painting analysis. part 1: pigment characterization, Herit. Sci. 11 (2023) 76-22, doi:10.1186/s40494-023-00910-x.

[32] Saunders D., Kirby J. The effect of relative humidity on artists' pigments. National Gallery Technical Bulletin Vol 25; 2004.

[33] L. Simonot, M. Elias, Color change due to surface state modification, Color Res. Appl. 28 (2003) 45–49, doi:10.1002/col.10113.

[34] F. Daniel, A. Mounier, J. Pérez-Arantegui, et al., Hyperspectral imaging applied to the analysis of Goya paintings in the museum of Zaragoza (Spain), Microchem. J. 126 (2016) 113–120, doi:10.1016/j.microc.2015.11.044.

[35] R. Radpour, G.A. Gates, I. Kakoulli, J.K. Delaney, Identification and mapping of ancient pigments in a roman Egyptian funerary portrait by application of reflectance and luminescence imaging spectroscopy, Herit. Sci. 10 (2022) 1–16, doi:10.1186/s40494-021-00639-5.

[36] J.K. Delaney, K.A. Dooley, A. van Loon, A. Vandivere, Mapping the pigment distribution of vermeer's girl with a pearl earring, Herit. Sci. 8 (2020) 1–16, doi:10.1186/s40494-019-0348-9.

[37] A. Polak, T. Kelman, P. Murray, et al., Hyperspectral imaging combined with data classification techniques as an aid for artwork authentication, J. Cult. Herit. 26 (2017) 1–11, doi:10.1016/j.culher.2017.01.013.

[38] L. Qi, J. Li, Y. Wang, M. Lei, X. Gao, Deep spectral convolution network for hyperspectral image unmixing with spectral library, Signal Process. 176 (2020) 107672, doi:10.1016/j.sigpro.2020.107672.

[39] L. Qi, F. Gao, J. Dong, X. Gao, Q. Du, SSCU-net: spatial-spectral collaborative unmixing network for hyperspectral images, TGRS 60 (2022) 1–15, doi:10.1109/TGRS.2022.3150970.

[40] B. Rasti, B. Koirala, P. Scheunders, J. Chanussot, MiSiCNet: minimum simplex convolutional network for deep hyperspectral unmixing, TGRS 60 (2022) 1–15, doi:10.1109/TGRS.2022.3146904.

[41] T. Kleynhans, C.M. Schmidt Patterson, K.A. Dooley, D.W. Messinger, J.K. Delaney, An alternative approach to mapping pigments in paintings with hyperspectral reflectance image cubes using artificial intelligence, Herit. Sci. 8 (2020) 1–16, doi:10.1186/s40494-020-00427-7.

[42] J.K. Delaney, J.G. Zeibel, M. Thoury, et al., Visible and infrared imaging spectroscopy of picasso's harlequin musician: mapping and identification of artist materials *in situ*, Appl. Spectrosc. 64 (2010) 584–594, doi:10.1366/000370210791414443.

[43] J.K. Delaney, M. Thoury, J.G. Zeibel, P. Ricciardi, K. Morales, K.A. Dooley, Visible and infrared imaging spectroscopy of paintings and improved reflectography, Herit. Sci. 4 (2016), doi:10.1186/s40494-016-0075-4.

[44] L.F. López, I.C. Blanco, M.F.S. Martín, M.L.V. de Ágredos Pasqual, L. Carlyle, J. Wadum, Paintings on copper and other metal plates: production, degradation and conservation issues, 2017 Colección UPV Scientia.

[45] K. Donahue-Wallace, The materials and techniques of european paintings on copper supports, in: Copper As Canvas: Two Centuries of Masterpiece Paintings On Copper, JSTOR, 1999, pp. 1575–1775.

[46] F. Pacheco, El arte de la pintura: su antigüedad y grandeza, Simon Faxardo, 1649.

[47] D. Vega, I. Pombo Cardoso, L. Carlyle, Pintura Sobre cobre: Investigación sobre Materiales y Técnicas De Aplicación De La Capa De Preparación a Través De Los Tratados Tradicionales y Estudio Analítico De Dos Obras Atribuidas a Las Escuelas Portuguesa y Flamenca, Conservar Patrimonio, 2018.

[48] R. Blanc, E. Manzano, A. López-Montes, N. Domínguez-Gasca, J.L. Vílchez, Non-invasive study of the pigments of a painting on copper with the inscription

"Boceto di pablo veronese" on the back, Heritage 6 (2023) 4787–4801, doi:10.3390/heritage6060254.

[49] Burns S.A. Subtractive color mixture computation. arXiv preprint arXiv:1710.06364. 2017.

[50] C. Chang, A. Plaza, A fast iterative algorithm for implementation of pixel purity index, IEEE Geosci. Remote Sens. Lett. 3 (2006) 63–67, doi:10.1109/LGRS.2005.856701.

[51] L. Simonot, M. Hébert, Between additive and subtractive color mixings: intermediate mixing models, JOSA A 31 (2014) 58–66, doi:10.1364/JOSAA.31.000058.

[52] F.A. Potra, S.J. Wright, Interior-point methods, J. Comput. Appl. Math. 124 (2000) 281–302, doi:10.1016/S0377-0427(00)00433-7.

[53] J. Romero, A. Garciá-Beltrán, J. Hernández-Andrés, Linear bases for representation of natural and artificial illuminants, J. Opt. Soc. Am. A Opt. Image Sci. Vis. 14 (1997) 1007, doi:10.1364/JOSAA.14.001007.

[54] Boardman J.W., Kruse F.A., Green R.O. Mapping target signatures *via* partial unmixing of AVIRIS data. Legacy CDMS: Jan 23, 1995. Available from: https://ntrs.nasa.gov/citations/19950027316.

[55] Boardman J.W. Automating spectral unmixing of AVIRIS data using convex geometry concepts. Legacy CDMS: Oct 25, 1993. Available from: https://ntrs.nasa.gov/citations/19950017428.

[56] M.A. Veganzones, M. Grana, in: Endmember Extraction Methods: A Short Review, Springer, 2008, pp. 400–407.

[57] R.A. Borsoi, T. Imbiriba, J.C.M. Bermudez, et al., Spectral variability in hyperspectral data unmixing: a comprehensive review, 2023 (accessed on 18/07/2023). https://github.com/ricardoborsoi/unmixing_spectral_variability/tree/master/methods/DeepGUn.

[58] L. Ortiz-Herrero, I. Cardaba, L. Bartolomé, M.L. Alonso, M.I. Maguregui, Extension study of a statistical age prediction model for acrylic paints, Polym. Degrad. Stab. 179 (2020) 109263, doi:10.1016/j.polymdegradstab.2020.109263.